

IDENTIFICATION OF BLAZAR CANDIDATES BEHIND SMALL AND LARGE MAGELLANIC CLOUDS

NATALIA ŻYWUCKA¹, ARTI GOYAL¹, MAREK JAMROZY¹, ŁUKASZ STAWARZ¹, MICHAŁ OSTROWSKI¹,
SZYMON KOZŁOWSKI², AND ANDRZEJ UDALSKI²

Draft version August 7, 2021

ABSTRACT

We report the identification of blazar candidates behind the Magellanic Clouds. The objects were selected from the Magellanic Quasars Survey (MQS), which targeted the entire Large Magellanic Cloud (LMC) and 70% of the Small Magellanic Cloud (SMC). Among the 758 MQS quasars and 898 of unidentified (featureless spectra) objects, we identified a sample of 44 blazar candidates, including 27 flat spectrum radio quasars and 17 BL Lacertae objects, respectively. All the blazar candidates from our sample were identified with respect to their radio, optical, and mid-infrared properties. The newly selected blazar candidates possess the long-term, multi-colour photometric data from the Optical Gravitational Lensing Experiment, multi-colour mid-infrared observations, and archival radio data for one frequency at least. In addition, for nine of them the radio polarization data are available. With such data, these objects can be used to study the physics behind the blazar variability detected in the optical and mid-infrared bands, as a tool to investigate magnetic field geometry of the LMC and SMC, and as an exemplary sample of point like sources most likely detectable in γ -ray range with the newly emerging Cherenkov Telescope Array.

Keywords: galaxies: active — galaxies: jets — BL Lacertae objects: general — Magellanic Clouds — quasars: general — radio continuum: galaxies

1. INTRODUCTION

Highly polarized (the degree of optical linear polarization $PD_o > 3\%$, Angel & Stockman 1980) flat-spectrum radio quasars (FSRQs) and BL Lacertae objects (BL Lacs) constitute a class of active galactic nuclei (AGN) called “blazars”, whose total radiative energy output is dominated by the Doppler-boosted, non-thermal emission from relativistic jets launched by accreting super-massive black holes from the centers of massive elliptical galaxies (e.g., Angel & Stockman 1980; Begelman et al. 1984; Urry & Padovani 1995). Blazars of the FSRQ type exhibit in addition prominent emission lines in their optical spectra due to the thermal plasma contribution; such lines are weak or even absent in the BL Lac subclass. The broad-band spectral energy distribution (SED) of blazar sources is characterized by two prominent peaks where, in the framework of the *lepton* scenario, the radio-to-optical/X-ray segment is believed to originate from the synchrotron radiation of electron-positron pairs accelerated up to TeV energies, while the high frequency X-ray-to- γ -ray segment is due to the Inverse Compton scattering of various ambient photon fields (produced both internally and externally to the outflow) by the jet electrons (Ghisellini et al. 1998). Alternatively, the hadronic scenario explains the broad-band continuum emission of blazars by assuming that protons, accelerated to ultra high energies (≥ 1 EeV), produce γ -rays via either the direct synchrotron emission or a meson decay and the synchrotron emission of secondaries from proton-photon interactions (e.g., Böttcher et al. 2013).

Based on the position of the synchrotron peak fre-

quency, ν_{peak} in the νF_ν plane, where F_ν is the observed energy flux spectral density, BL Lacs can be further divided into low frequency peaked BL Lacs (LBLs; $\nu_{\text{peak}} \lesssim 10^{14}$ Hz), intermediate frequency peaked BL Lacs (IBLs; $10^{14} \lesssim \nu_{\text{peak}} \lesssim 10^{15}$ Hz), and high frequency peaked BL Lacs (HBLs; $\nu_{\text{peak}} \gtrsim 10^{15}$ Hz; Abdo et al. 2010b). FSRQs are characterized by $\nu_{\text{peak}} < 10^{14}$ Hz but larger peak intensity ratio between the Inverse Compton and synchrotron emission components (aka the “Compton dominance”) when compared with the LBLs. The so called *blazar sequence* formed by the decreasing ν_{peak} with the increasing Compton dominance, was proposed to result from stronger and stronger radiative cooling suffered by the emitting electrons due to the increasing energy density of the seed photon population for the Inverse Compton scattering (e.g., Ghisellini et al. 1998; Fossati et al. 1998; Ghisellini & Tavecchio 2008).

Blazars are the ideal candidates to test the extreme physics of relativistic jets, due to their large observed luminosities $\lesssim 10^{48}$ ergs s^{-1} (Ghisellini et al. 2014) and high-amplitude intensity changes on various timescales from years down to minutes (Cui 2004; Aharonian et al. 2007; Ackermann et al. 2016b), as well as to examine their evolution and large scale structure formation (Ackermann et al. 2017). Blazars show the most extreme behavior in the radio-optical polarization variability on different timescales, ranging from years to minutes, among all the AGN. The polarization at radio frequencies is weaker than in the optical bands with the characteristic radio linear polarization degree $PD_{r,1.4} > 1\%$ at 1.4 GHz (Iler et al. 1997). Fan et al. (2008) showed that the polarization is linked to the amount of relativistic beaming, that the averaged polarization increases with the radio frequency for FSRQs, and that, statistically, radio-selected BL Lacs are more polarized than FSRQs. Polarimetric observations can be used as a tool to study

n.zywucka@oa.uj.edu.pl

¹ Astronomical Observatory of the Jagiellonian University, ul. Orła 171, 30-244 Kraków, Poland

² Astronomical Observatory of the University of Warsaw, Al. Ujazdowskie 4, 00-478 Warszawa, Poland

the location of the emission regions in blazar jets (e.g., Jorstad et al. 2007; Blinov 2009; Zhang et al. 2016), to constrain the structure of the jet magnetic field (e.g., Aller et al. 2003; Marscher 2014), and to probe the interstellar medium of foreground galaxies via the Faraday rotation measure method (RM; e.g., Gaensler et al. 2005; Mao et al. 2012).

In the present study, we report the identification of blazar candidates behind the LMC and SMC which are selected from the catalogue of the Magellanic Quasar Survey (MQS; Kozłowski et al. 2013) and a “featureless spectra” (FS) objects list (Section 2). In Section 3 we shortly describe the optical, mid-IR, and radio data sets analyzed, while Section 4 contains details of the selection and identification procedures. The main results of the studies are discussed in the final Section 5.

2. INPUT SAMPLE SELECTION

The AGN identification based on the optical colour selection is extremely challenging in dense stellar fields such as the Galactic plane or LMC and SMC, due to large densities of stars ($\sim 10^6 \text{ deg}^{-2}$) in the interstellar medium as compared to quasars ($\sim 25 \text{ deg}^{-2}$) from the background, for a limiting magnitude $I < 20$. With the main goal of studying the optical variability of quasar light curves based on the Optical Gravitational lensing Experiment (OGLE)-III phase (Udalski et al. 2008a,b), the MQS survey was designed to increase the number of the identified AGN behind both Magellanic Clouds (MCs). This survey covers 42 deg^2 in the sky and completed 100% and 70% of its planned LMC and SMC areas, respectively. Below, we briefly recall the step-by-step AGN selection procedure that led to the MQS input sample (see, Kozłowski & Kochanek 2009; Kozłowski et al. 2010, 2011, 2012, 2013).

2.1. The MQS catalogue

The MQS quasar candidates were identified in the four-step selection procedure which involves: (i) mid-infrared (mid-IR) properties, (ii) optical variability, (iii) ROSAT X-ray sources’ counterparts, and (vi) optical spectroscopy study:

- (i) Kozłowski & Kochanek (2009) identified 4,699 and 657 quasar candidates in the LMC and SMC, respectively. These quasar candidates were selected based on the mid-IR and optical colour-colour selection by cross-matching the mid-IR data from the Spitzer SAGE Survey data (Meixner et al. 2006) and the S3MC Survey (Bolatto et al. 2007), and the OGLE-III optical survey. As a result, mid-IR colour-colour, mid-IR colour-magnitude, and mid-IR-to-optical colour planes were created in order to separate AGN from stars, young stellar objects (YSOs), planetary nebulae (PNe), and other galactic and extragalactic sources. The selected sample was further divided into the QSO and YSO groups and subgroups. All of them may contain quasars, as well as other sources, but only the QSO-Aa group is considered to include the highest number of AGN, while the other groups are mostly populated by contaminating sources (Kozłowski & Kochanek 2009).
- (ii) The OGLE-III light curves were analyzed using the damped random walk (DRW) model (Kelly et al.

2009; Kozłowski et al. 2010) and the structure function (SF) method (Kozłowski 2016). The DRW model fits the light curve as a stochastic process with exponential covariance matrix characterized by the two parameters: a damping time scale τ and an amplitude of the driving Gaussian noise σ . Kozłowski et al. (2010) showed that quasars occupy a well defined locus in the σ - τ space, where over 1,000 quasar candidates were selected for the MQS input sample.

- (iii) The LMC and SMC OGLE variable source positions were cross-matched with the ROSAT catalogues (Haberl & Pietsch 1999; Haberl et al. 2000) to find any X-ray counterparts at the level of 3σ . As a result, a small sample of 205 X-ray detected candidates was selected (Kozłowski et al. 2012).
- (iv) The final confirmation whether an object is a quasar or not was based on spectroscopic observations of 3,014 sources, including 2,248 behind the LMC and 766 behind the SMC, selected according to at least one of the (i)–(iii) methods. The spectroscopic data were obtained using the 3.9 m Anglo-Australian Telescope (AAT) and the AAOmega spectrograph. Only the sources with at least two visible emission lines in each spectrum, except for the objects at the redshifts between 0.7 and 1.2 (where only Mg II line is visible), were used for the AGN identification. In such a manner, Kozłowski et al. (2013) confirmed spectroscopically 565 quasars in the LMC and 193 quasars in the SMC, totalling 758 sources in the MQS catalogue.

Prior to the MQS survey, only 66 quasars were known behind the MCs. Owing to all the aforementioned selection criteria, 758 quasars were selected from the OGLE data, including 713 newly identified quasars: 565 (within which 527 are new) and 193 (186), behind the LMC and SMC, respectively. For all spectroscopically observed MQS objects there exist long-term, densely sampled optical light curves from the OGLE survey.

2.2. The FS list

The spectroscopic observations also resulted in 898 objects (669 in the LMC and 229 in the SMC fields) without any distinguishing features in their spectra, either intrinsically or due to a low S/N statistics for the line detection. These objects could be associated with either BL Lac type blazars, or OB stars, YSOs, PNe, and other types of Galactic or extragalactic objects.

3. MULTIWAVELENGTH OBSERVATIONS

3.1. Mid-IR data

3.1.1. Wide Infrared Survey Explorer

The Wide-field Infrared Survey Explorer (WISE) is a satellite launched in December 2009 and designed to map the entire sky and to monitor individual astrophysical objects in mid-IR range. This 40 cm diameter telescope is equipped with IR detectors collecting data in four bands centered at 3.4 (W1), 4.6 (W2), 12 (W3), and 22 (W4) μm with the angular resolutions of $6''1$, $6''4$, $6''5$, and $12''0$, respectively (Wright et al. 2010).

Table 1
Summary of radio catalogues and surveys used in this study.

Survey	Telescope	Frequency [GHz]	Area	beam size ["]	rms [mJy/beam]
(1)	(2)	(3)	(4)	(5)	(6)
SUMSS ¹	MOST	0.843	$\delta \leq -30$	$43 \times 43 \text{ cosec} \delta $	$1 \div 2$
AT20G ²	ATCA	5, 8, 20	$\delta \leq -15$	9.9, 5.5, 2.4	$0.1 \div 0.5$
PMN ³	Parkes 64 m	4.85	$\delta \leq 10$	252	$5 \div 7$
ATPMN ⁴	ATCA	4.8, 6.8	$-87 < \delta < -38$	1.8, 1.2	$15 \div 20$
SMC multi ⁵	ATCA and Parkes	$1.42 \div 8.64$	100% of SMC	$98 \div 15$	$1.8 \div 0.4$
LMC dual ⁶	ATCA	4.8, 8.6	100% of LMC	33, 20	0.1
SMC dual ⁷	ATCA	4.8, 8.6	100% of SMC	35, 22	0.15

Note. — ¹Bock et al. 1999; ²Murphy et al. 2010; ³Griffith & Wright 1993; ⁴McConnell et al. 2012; ⁵Filipović et al. 2002; ⁶Dickel et al. 2005; ⁷Dickel et al. 2010

Columns: (1) name of sky survey; (2) telescope used; (3) central frequency of observations; (4) sky coverage; (5) typical resolution (beam size) achieved; (6) typical noise level.

3.1.2. SAGE LMC and SMC IRAC Source Catalogues

Both the LMC and SMC regions were observed using the four-band Infrared Array Camera (IRAC) and the three-band Multiband Imaging Photometer for SIRTE (MIPS) instruments, on-board the Spitzer Space Telescope (Werner et al. 2004), as a part of the program Surveying the Agents of a Galaxy’s Evolution (SAGE³ Meixner et al. 2006; Gordon et al. 2011). The angular resolution is $1''.7$, $1''.7$, $1''.9$, and $2''.0$ in the IRAC bands, centered at 3.6, 4.5, 5.8, and 8.0 μm , respectively, while it is $6''.0$, $18''.0$, and $40''.0$ in the MIPS bands centered at 24, 70, and 160 μm , respectively. In our study, we have used the simultaneous IRAC data only, in order to minimize uncertainties of the selection procedure.

3.2. Radio continuum surveys

Self-absorbed radio cores and the high degree of optical polarization are the defining characteristics of blazars (e.g., Blandford & Königl 1979). Therefore, in order to ascertain the blazar nature of sources from the MQS and the FS lists, we searched for radio counterparts of the optically detected sources in various radio sky surveys and catalogues. Description of the sky surveys and catalogues are given below and their main characteristics are listed in Table 1.

3.2.1. The SUMSS catalogue

The SUMSS sky survey (Bock et al. 1999) was performed with the Molonglo Observatory Synthesis Telescope (MOST) and covered 2.47 sr of the southern sky with $\delta \leq -30^\circ$ at the frequency of 0.843 GHz. The observations were completed in 2007 and are publicly available⁴. The SUMSS catalogue consists of 210,412 radio sources with the peak brightness limit of 6 mJy/beam at $\delta \leq -50^\circ$ and 10 mJy/beam at $\delta > -50^\circ$. The synthesized beam of the maps is $43'' \times 43'' \text{ cosec}|\delta|$. The position accuracy of the radio sources in the catalogue are within $1\text{--}2''$ for the objects with the peak fluxes ≥ 20 mJy/beam, while for the remaining sources with lower radio fluxes, the position accuracy is not worse than $10''$.

3.2.2. The AT20G catalogue

The AT20G sky survey (Murphy et al. 2010) was conducted between 2004 and 2008 with the Australia Telescope Compact Array (ATCA) and covered 6.12 sr of the southern sky ($\delta < 0^\circ$). The AT20G catalogue contains 5,890 radio sources with the flux-density limit of 40 mJy. Near-simultaneous measurements at 5 and 8 GHz south of $\delta < -15^\circ$ were also performed. The synthesized beam of this sky survey is $2''.4$, $5''.5$, and $9''.9$ at the frequencies of 20, 8, and 5 GHz, respectively. In addition, the total polarized intensity was measured and collected in the catalogue for 1,559 sources at one up to three frequencies.

3.2.3. The PMN catalogue

The PMN sky survey (Griffith & Wright 1993; Wright et al. 1994) of the southern hemisphere was performed in 1990 with the Parkes 64 m telescope at 4.85 GHz and covered the sky region of $-87.5^\circ < \delta < +10^\circ$. The radio survey was conducted in four areas and divided into the following subparts: Southern with the declination of $-87.5^\circ < \delta < -37^\circ$, Zenith with $-37^\circ < \delta < -29^\circ$, Tropical $-29^\circ < \delta < -9.5^\circ$, and Equatorial with $-9.5^\circ < \delta < +10^\circ$. The resolution of the survey is $252''$. The PMN catalogue consists of 50,814 radio sources including 23,277 sources of the Southern Survey. The flux density limit varies between 50 mJy/beam at the northern edge ($\delta \approx -37^\circ$) and 20 mJy/beam at the southern edge of this region.

3.2.4. The ATPMN catalogue

The ATPMN follow-up catalogue (McConnell et al. 2012) is a result of observations of PMN sources with the ATCA. The data were carried out at 4.8 and 8.6 GHz and covered the region of 2.25 sr ($-87^\circ < \delta < -38.5^\circ$). The ATPMN catalogue consists of 9,040 sources with the flux density of 70 mJy/beam at $\delta > -73^\circ$ and 50 mJy/beam at $\delta \leq -73^\circ$. The angular resolution of the ATPMN radio survey is high and varies between $1''.2$ and $1''.8$.

3.2.5. The ATCA/Parkes SMC survey

The ATCA radio-continuum study of the SMC was performed by Filipović et al. (2002) based on the observations by the ATCA and the Parkes 64 m telescopes. The catalogues contain 717 radio sources detected in the SMC at 1.42, 2.37, 4.8, and 8.64 GHz. The beam size varies from $98''$ at 1.42 GHz to $15''$ at 8.64 GHz, and the positional accuracy is less than $1''$.

³ <http://sage.stsci.edu/>

⁴ <http://www.physics.usyd.edu.au/sifa/Main/SUMSS>

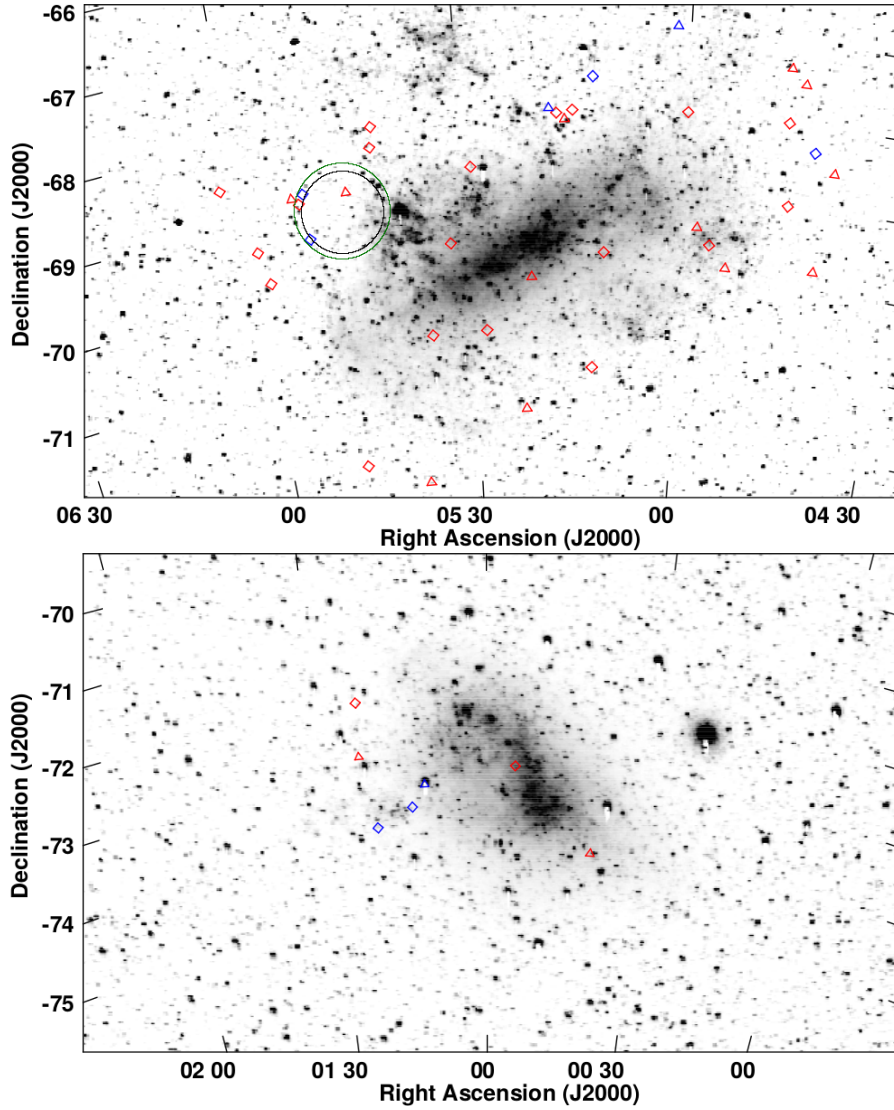


Figure 1. Distribution of the selected blazar candidates behind the LMC (top panel) and SMC (bottom panel). The optical positions of the FSRQ candidates are shown with red diamond symbols, while red triangular symbols denote the BL Lac candidates. Objects with polarimetric measurements are additionally marked with blue symbols. Black and green circles show possible areas of the γ -ray flaring activity detected by the *Fermi*-LAT during the 4th month of observations and, later, in April 2015 (see, Section 4.6). The optical images of both MC (grey scale) are taken from [Bothun & Thompson \(1988\)](#).

3.2.6. The 4.8 and 8.6 GHz Survey of the MCs

The 4.8 and 8.6 GHz Surveys of LMC (Dickel et al. 2005) and SMC (Dickel et al. 2010) were performed using the ATCA and the Parkes 64 m telescopes. The work was intended to study a diffuse emission in the Galaxy, supernova remnants and HII regions, as well as bright point sources. The simultaneous observations of the total intensity and the polarized flux density at 4.8 and 8.6 GHz were gathered to produce $6^\circ \times 6^\circ$ maps with the resolutions of $33''$ and $20''$ at 4.8 and 8.6 GHz, respectively, for the LMC, and $4.5^\circ \times 4.5^\circ$ maps with the resolutions of $35''$ and $22''$ at 4.8 and 8.6 GHz, respectively, for the SMC. In our work, we have used the maps obtained with the ATCA array only, since the Parkes 64 m telescope is suitable for extended radio emission. Since no catalogue has resulted from these surveys, we have measured the total intensity and polarized fluxes directly from the maps provided by Dickel et al. (2005)⁵ and Dickel et al. (2010)⁶.

4. IDENTIFICATION OF BLAZAR CANDIDATES

As stated earlier, the MQS catalogue contains 758 quasars. Statistically, around 10–15% of them (i.e., 75–110) should be “radio-loud”, meaning the ratio of radio 5 GHz to optical B-band flux spectral densities $R \equiv F_{5\text{GHz}}/F_B \geq 10$ (Kellermann et al. 1989; Stocke et al. 1992; Ho 2002). Among those radio-loud quasars, at least *some* ($\lesssim 10\%$; see, e.g., Ghisellini et al. 2013) should be blazars of the FSRQ type. The FS list, on the other hand, may contain BL Lac type blazars, which should be radio-loud as well.

The blazar candidates from both lists are, therefore, selected using the radio and optical positioning, i.e., the cross-matching procedure. The identified sample of blazar candidates is further analyzed by investigating characteristic radio, mid-IR, and optical properties of the sources, such as spectral radio and mid-IR indices, radio-loudness parameter, and fractional linear polarization.

4.1. Cross-matching of source positions

We searched for the radio counterparts by cross-matching the optical positions of the MQS and FS sources with the positions of radio sources listed in the radio catalogues with the standard spherical trigonometric distance procedure. In particular, we defined the radius Δr of the error circle as:

$$\Delta r = \sqrt{\left(\frac{1}{3} r_{b_1}\right)^2 + \left(\frac{1}{3} r_{b_2}\right)^2} \quad (1)$$

where r_{b_1} is the resolution of the OGLE catalogue and r_{b_2} is the angular resolution of various radio catalogues considered. With such, the radio counterpart was considered to be coincident with the optical source if their spherical distance was found to be equal or less than Δr .

Out of the 758 AGN in the MQS catalogue, 17 were found to have measured radio fluxes at more than one radio frequency, 10 at one frequency only, and the remaining 731 quasars could not be matched with any radio counterparts. Similarly, out of the 898 sources in the FS

list, seven were found to have measured radio fluxes at more than one frequency, 10 at one frequency, while 881 sources have no radio counterparts. All the sources identified in the cross-matching procedure along with their radio fluxes are reported in Table 2. These are termed hereafter as “blazar candidates” and are further summarized in Table 3. Figure 1 presents the overlays of the optical images of the both MCs with the positions of blazar candidates.

4.2. Radio indices, radio-loudness, and redshifts

For the newly selected blazar candidates, we estimate the radio spectral indices α_r , defined here as $F_\nu \propto \nu^{-\alpha_r}$. The radio spectral index value indicates whether a radio spectrum of a source is flat ($\alpha_r < 0.5$) or steep ($\alpha_r > 0.5$). Flat radio spectra are the defining characteristics of blazars, as mentioned previously. It is noteworthy here that blazars are extremely variable objects, hence simultaneous observations are needed to calculate the robust values of radio spectral indices. In this work, we are, however, forced to rely on the α_r values estimated based on non-simultaneous data. The radio indices were calculated for the selected objects, which possess at least two measurements at different frequencies available in the aforementioned data sets. The radio flux spectral densities at different frequencies and resulting α_r values are presented in Table 2 and Table 3, respectively.

We have also estimated the values of the radio-loudness parameter R for our blazar candidates, as listed in Table 3. Since the radio data at exact 5 GHz were available for four sources only, i.e., two FSRQ and two BL Lac blazar candidates, when estimating the R values, we have extrapolated radio fluxes from lower frequencies assuming the radio spectral index as $\alpha_r = 0.5$. The R distributions for the blazar candidates (red dashed line) are shown in Figure 2. For comparison, we have also included in the histograms the upper limits on R (black solid line) estimated for the remaining objects from both lists based on the 5 GHz ATCA flux upper limit.

As shown in the figure, our sample of blazar candidates consists of the sources characterized by the highest values of R , among both the MQS and FS lists. Note, however, that due to relatively high flux limits of the radio surveys considered (when compared to the optical flux limit of the OGLE project), many quasars from the MQS catalogue which have not been matched here with any radio counterpart, could still be radio-loud, as the upper limits for the R parameter for the majority of such sources are rather high, namely $R < 100$. Hence, our sample of blazar candidates does not contradict the expectation for 10%–15% of the MQS quasars being radio-loud; instead, Figure 2 indicates only that our selection procedure picks up $\sim 3.6\%$ of the most radio-loud quasars from the MQS sample, roughly in agreement with what is expected for the beamed (blazar) population in the parent population of quasars.

Figure 3 shows the z distribution of the MQS quasars (black solid line) and the FSRQ blazar candidates (red dashed line). Among ~ 10 MQS quasars at $z > 3$, we have selected one blazar candidate, i.e. J0528-6836 with $z = 3.32$.

⁵ http://www.atnf.csiro.au/research/lmc_ctm/index.html

⁶ http://www.atnf.csiro.au/research/smc_ctm/index.html

Table 2
The radio fluxes of FSRQ type blazar candidates.

Object	F _{0.84} [mJy]	F _{1.42} [mJy]	F _{2.37} [mJy]	F _{4.8} [mJy]	F _{4.85} [mJy]	F _{5.0} [mJy]	F _{8.0} [mJy]	F _{8.6} [mJy]	F _{20.0} [mJy]
(1)	(2)	(3)	(4)	(5)	(6)	(7)	(8)	(9)	(10)
FSRQ blazar type candidates									
J0054–7248 ^a					36.0±6.0				
J0114–7320	129.0±4.0	86.8±4.3	70.3±3.5	19.0±7.0				15.0±10.0	
				18.5±1.1 ^e				17.4±1.5 ^e	
				288.0±14.4				22.0±1.1	
J0120–7334	56.2±3.0	45.8±2.3	31.6±1.6	24.0±1.4 ^e	29.0±6.0			15.3±1.2 ^e	
J0122–7152	6.8±1.0								
J0442–6818	9.2±1.0				29.0±7.0	51.0±3.0	60.0±4.0		74.0±4.0
J0445–6859	25.3±1.7								
J0446–6758	6.0±0.8								
J0455–6933	80.4±4.0			36.5±2.0 ^e		17.0±7.0		27.0±1.8 ^e	
J0459–6756 ^a					34.0±7.0				
J0510–6941	31.2±1.3			8.9±0.8 ^e				6.2±2.0 ^e	
J0512–7105	11.0±0.9			2.8±0.7 ^e					
J0512–6732	59.2±2.2			45.7±2.4 ^e		47.0±2.0	56.0±3.0	48.5±2.6 ^e	46.0±3.0
J0515–6756 ^a					27.0±7.0				
J0517–6759 ^a					29.0±7.0				
J0527–7036	137.8±4.2			34.0±7.0				11.0±10.0	
				39.8±2.1 ^e				24.7±1.5 ^e	
J0528–6836	31.1±1.5			31.1±1.7 ^e	49.0±7.0			22.7±1.4 ^e	
J0532–6931	10.3±1.3			12.6±2.6 ^e					
J0535–7037 ^a					35.0±7.0				
J0541–6800	54.5±1.9			45.7±2.4 ^e	59.0±7.0			32.3±1.8 ^e	
J0541–6815	45.8±1.6			48.8±2.5 ^e				38.8±2.1 ^e	
J0547–7207	24.6±1.9			8.0±0.9 ^e				7.1±1.8 ^e	
J0551–6916				32.9±1.8 ^e	35.0±7.0			14.8±1.2 ^e	
J0551–6843	158.5±6.4			32.6±0.8 ^e				14.0±1.8 ^e	
J0552–6850 ^a					49.0±7.0				
J0557–6944	49.0±1.7				40.0±7.0				
J0559–6920 ^a					27.0±7.0				
J0602–6830	52.0±1.7				40.0±7.0				
BL Lac type blazar candidates									
J0039–7356	8.5±1.1		4.2±0.2						
J0111–7302	86.4±4.2	111.5±5.6	77.4±3.9	69.0±7.0	72.0±7.0	72.0±4.0	72.0±4.0	61.0±10.0	74.0±4.0
				62.9±3.2 ^e				53.6±2.8 ^e	
J0123–7236	10.8±0.9		4.6±0.2						
J0439–6832	36.2±1.4								
J0441–6945	59.4±3.0								
J0444–6729	34.3±1.3								
J0446–6718	9.9±1.1								
J0453–6949	6.2±0.9								
J0457–6920 ^a					30.0±7.0				
J0501–6653	51.7±1.8			17.7±1.1 ^e				9.7±1.0 ^e	
J0516–6803 ^a				29.0±7.0					
J0518–6755 ^a				67.71±3.5 ^e	95.0±8.0			33.40±2.0 ^e	
J0521–6959 ^a				52.6±2.7 ^e	58.0±7.0			29.3±2.0 ^e	
J0522–7135 ^a					89.0±8.0				
J0538–7225	7.0±1.0								
J0545–6846	176.3±7.4			41.7±2.2 ^e	26.0±7.0			23.1±1.7 ^e	
J0553–6845	22.2±1.1								

Note. — ^aDubious objects; Columns: (1) source designation, (2) - (10) radio flux density at 0.843, 1.42, 2.37, 4.8, 4.85, 5.0, 8.0, 8.6, and 20.0 GHz, respectively; ^e radio flux measurements based on the 4.8 and 8.6 GHz radio surveys of the MCs.

Table 3
Newly identified FSRQ and BL Lac type blazar candidates.

Object	RA	DEC	R	z	α_r	α_{IR}	I [mag]
(1)	(2)	(3)	(4)	(5)	(6)	(7)	(8)
FSRQ type blazar candidates							
J0054–7248 ^a	00 54 44.70	-72 48 13.68	1730	0.505		1.89±0.50	20.73
J0114–7320	01 14 05.57	-73 20 06.50	246	0.937	0.58±0.31	1.33±0.13	18.26
J0120–7334	01 20 56.05	-73 34 53.51	195	1.565	0.56±0.06	1.88±0.07	17.66
J0122–7152	01 22 58.49	-71 52 07.00	267	0.939		0.47±0.18	19.84
J0442–6818	04 42 45.19	-68 18 38.99	371	0.964	-0.57±0.15	1.20±0.09	18.22
J0445–6859	04 45 36.60	-68 59 46.10	285	1.714		1.73±0.02	18.87
J0446–6758	04 46 33.91	-67 58 55.88	169	1.301		1.72±0.15	19.96
J0455–6933	04 55 59.10	-69 33 29.09	336	1.319	0.47±0.04	1.30±0.06	18.78
J0459–6756 ^a	04 59 54.27	-67 56 35.59	898	1.687		1.45±0.14	19.29
J0510–6941	05 10 45.85	-69 41 26.48	165	1.061	0.72±0.01	0.60±0.02	18.37
J0512–7105	05 12 21.49	-71 05 55.61	489	0.286	0.79±0.00	1.71±0.03	20.70
J0512–6732	05 12 22.48	-67 32 20.00	557	2.557	0.08±0.04	1.99±0.09	18.37
J0515–6756 ^a	05 15 03.49	-67 56 53.02	4440	0.374		1.83±0.05	20.20
J0517–6759 ^a	05 17 10.31	-67 59 01.21	4450	0.427		1.01±0.19	20.42
J0527–7036	05 27 49.08	-70 36 41.69	769	0.774	0.73±0.02	1.13±0.05	18.39
J0528–6836	05 28 47.51	-68 36 20.99	580	3.320	0.08±0.11	0.49±0.18	18.32
J0532–6931	05 32 12.24	-69 31 30.90	12	1.353	-0.12±0.00	1.39±0.04	16.54
J0535–7037 ^a	05 35 47.71	-70 37 50.70	2670	0.731		1.49±0.12	20.34
J0541–6800	05 41 34.97	-68 00 40.61	494	0.934	0.18±0.08	0.93±0.06	19.64
J0541–6815	05 41 58.96	-68 15 42.30	351	1.586	0.04±0.07	1.42±0.08	18.59
J0547–7207	05 47 58.68	-72 07 45.30	121	0.793	0.61±0.06	0.96±0.08	18.79
J0551–6916	05 51 33.21	-69 16 33.82	304	2.226	1.38±0.06	1.71±0.07	17.93
J0551–6843	05 51 40.55	-68 43 08.40	987	1.595	1.00±0.09	1.34±0.05	18.39
J0552–6850 ^a	05 52 22.53	-68 50 01.72	1970	1.740		1.57±0.02	19.34
J0557–6944	05 57 59.59	-69 44 12.19	1530	0.480	0.12±0.00	0.59±0.09	20.14
J0559–6920 ^a	05 59 01.63	-69 20 09.38	1050	1.817		1.66±0.21	19.54
J0602–6830	06 02 34.31	-68 30 41.40	356	1.086	0.23±0.00	1.37±0.10	18.39
BL Lac type blazar candidates							
J0039–7356	00 39 42.51	-73 56 15.50	1570		0.68±0.00	0.97±0.12	20.85
J0111–7302	01 11 33.24	-73 02 03.41	171		0.14±0.05		19.10
J0123–7236	01 23 17.47	-72 36 05.40	199		0.83±0.00	2.04±0.14	20.49
J0439–6832	04 39 50.17	-68 32 22.60	1030			1.34±0.15	20.21
J0441–6945	04 41 04.99	-69 45 40.72	3840			1.29±0.06	21.11
J0444–6729	04 44 55.57	-67 29 40.42	689			0.15±0.14	19.58
J0446–6718	04 46 55.72	-67 18 38.48	478			1.33±0.08	20.53
J0453–6949	04 53 29.83	-69 49 28.60	285			1.30±0.11	20.74
J0457–6920 ^a	04 57 50.55	-69 20 51.61	2040			1.65±0.44	19.93
J0501–6653	05 01 39.74	-66 53 53.48	1490		0.66±0.06	-0.44±0.17	19.37
J0516–6803 ^a	05 16 07.14	-68 03 37.30	1750			3.07±0.41	20.08
J0518–6755 ^a	05 18 09.01	-67 55 23.48	89		1.37±0.34	2.00±0.00	18.60
J0521–6959 ^a	05 21 00.02	-69 59 06.58	2010		1.03±0.11	1.51±0.24	19.18
J0522–7135 ^a	05 22 23.92	-71 35 31.30	7020			1.19±0.15	20.08
J0538–7225	05 38 16.96	-72 25 00.10	290			1.78±0.18	20.32
J0545–6846	05 45 51.78	-68 46 03.00	6900		0.86±0.04	0.81±0.08	21.27
J0553–6845	05 53 15.71	-68 45 27.20	3080			1.93±0.10	20.00

Note. — ^aDubious objects; Columns: (1) source designation, (2) right ascension (RA) in J2000.0, (3) declination (DEC) in J2000.0, (4) the radio-loudness R parameter, (5) redshift z , (6) radio spectral index α_r , (7) mid-IR spectral index α_{IR} , and (8) I band magnitude. The coordinates, z , and I band magnitude were taken from the MQS catalogue or FS list.

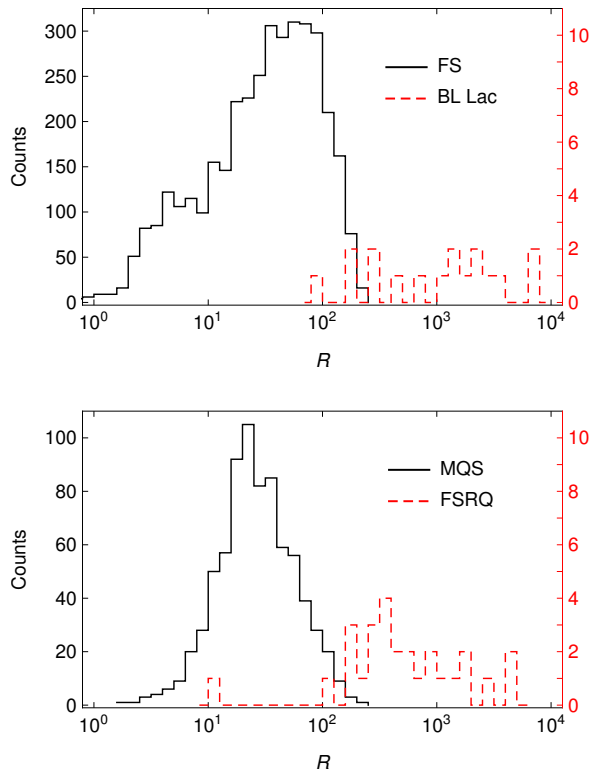


Figure 2. Radio-loudness distributions of the FSRQ (upper panel) and the BL Lac (bottom panel) type blazar candidates, shown by red dashed lines. Black solid lines correspond to the 5 GHz ATCA upper limits for the sources catalogued in the MQS or the FS lists.

4.3. Comparison with Roma-BZCAT

We compared our sample with 1,425 BL Lacs and blazar candidates and 1,909 FSRQs and blazar candidates listed in the 5th edition of the Roma-BZCAT: *Multi-frequency Catalogue of Blazars*⁷ (Roma-BZCAT, Massaro et al. 2015). The following parameters from Roma-BZCAT were taken into account in this investigation: the z distribution, radio flux densities at 1.4 GHz from the Faint Images of the Radio Sky at Twenty-cm (FIRST) or 0.843 GHz from the SUMSS catalogue (if not available in the former), and optical apparent magnitudes in R filter from the tenth Sloan Digital Sky Survey data release (SDSS DR10).

Figure 4 shows the z distributions of the OGLE FSRQ candidates (red dashed line) and the Roma-BZCAT FSRQs (black solid line). Note that 29 FSRQs, which are listed in the Roma-BZCAT catalogue with “?” symbol are not included in this study due to the uncertain z values.

The distributions of radio flux spectral densities of both blazar type candidates are presented in Figure 5. In case of the OGLE blazar candidates only the 0.843 GHz flux density measurements were used. Figure 6 shows the distributions of optical apparent magnitude in R filter of the Roma-BZCAT sources and in I filter of the OGLE blazar candidates (note the very similar effective wavelengths for both filters)

A Kolmogorov-Smirnov test (Massey 1951; Tarnopol-

⁷ <http://www.asdc.asi.it/bzcat>

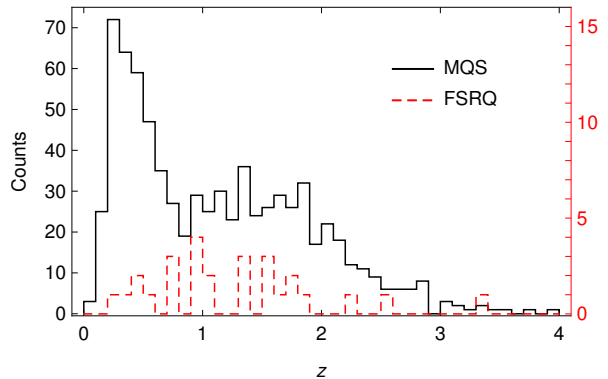


Figure 3. Redshift distributions of the MQS quasars. Black solid line shows the distribution of the quasars lacking radio counterparts, while red dashed line is for the FSRQ blazar candidates.

ski 2015) was performed to verify the null hypothesis, H_0 , whether the samples examined in this work have the same distributions as the corresponding datasets from Roma-BZCAT. Bear in mind, however, that the K-S test was used here to compare a small sample of newly identified blazar candidates, consisting of 12 up to 27 sources depending on the compared parameters, with a relatively large Roma-BZCAT sample. In the case of the redshift distribution of FSRQs, H_0 is not rejected at the $\alpha = 0.01$ significance level. For the radio flux distribution of BL Lacs, the H_0 is also not rejected, unlike in the case of radio flux distribution of FSRQs, for which the H_0 is rejected with the p -value = 6×10^{-11} . For the apparent magnitude distributions in I and R filters, H_0 hypothesis is not rejected for FSRQs, but is rejected for BL Lacs.

All in all, a comparison between the list of blazar candidates selected here and the Roma-BZCAT, indicates that even though the redshift and the apparent optical magnitude distributions of FSRQs in both samples are similar, our FSRQ candidates are characterized by lower radio fluxes, on average. In the case of BL Lacs, on the other hand, while the radio flux distributions seem comparable, the objects from our list appear on average dimmer in optical.

4.4. Mid-IR colours

The mid-IR colour criteria provide a useful tool enabling the identification of AGN among other objects, FSRQ

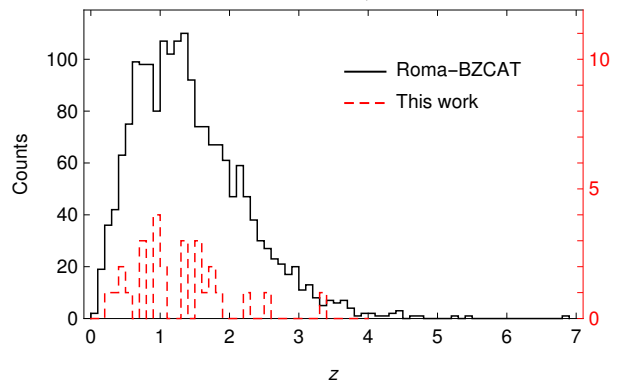


Figure 4. Redshift distributions of the FSRQ blazar candidates (red dashed line) and the FSRQ blazars from Roma-BZCAT (black solid line).

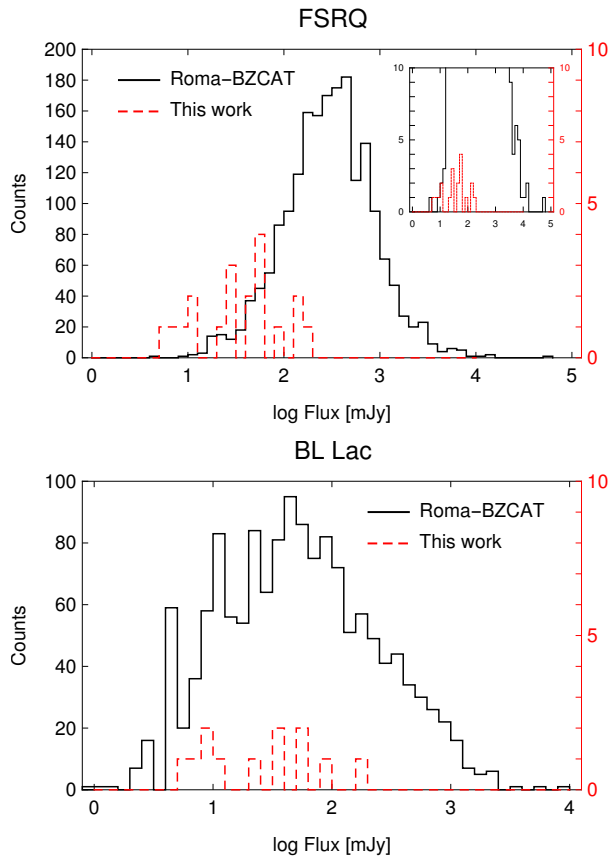


Figure 5. Distributions of 0.84 GHz flux of the FSRQ (upper panel) and BL Lac (bottom panel) blazars from Roma-BZCAT and blazar candidates identified in this work.

such as stars or normal galaxies. In particular, Stern et al. (2005) and later Massaro et al. (2011) and D’Abrusco et al. (2012) proposed diagnostic tools to separate blazars based on their IR colours.

We analyzed our sample of blazar candidates using the data collected by WISE and the Spitzer Space Telescope (the IRAC instrument), generating four mid-IR colour-colour planes, i.e. $[3.4]-[4.6]-[12]$ and $[3.4]-[4.6]-[12]-[22]$ μm based on the WISE observations (Figure 7), and $[3.6]-[4.5]-[8.0]$ μm and $[3.6]-[4.5]-[5.8]-[8.0]$ μm with the IRAC data (Figure 8). In the figures, black filled circles denote the mid-IR colours of the FSRQ blazar candidates, and black open circles indicate the mid-IR colours of the BL Lac candidates; black dashed lines correspond to the case of a single power-law emission continuum within the entire range of wavelength considered (e.g., $3.4-12$ μm in the upper panel of Figure 7, or $3.4-22$ μm in the lower panel of Figure 7), with the particular values of mid-IR spectral indices $\alpha = 0, 1$, and 2 denoted by \times symbols; finally, red open circles mark the BL Lac candidate J0545-6846, which coincides with the γ -ray transient detected by the *Fermi*-LAT (see Section 4.6).

Figure 7 displays in addition a comparison between our blazar candidates and 7,855 γ -ray blazar candidates (FSRQs, BL Lacs, and mixed-type objects, all denoted by small grey dots) selected based on the *All-WISE Data Release* products (Cutri et al. 2013) and listed in the *WISE blazar-like radio-loud sources* catalogue (WIBRaLS, D’Abrusco et al. 2014). Some of our blazar candidates occupy the same area in the plot as the

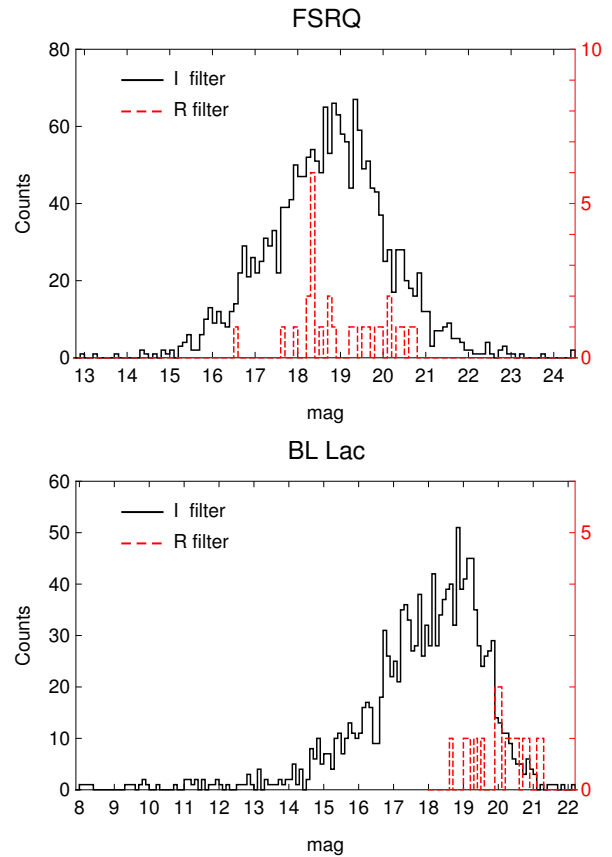


Figure 6. Distributions of R mag and apparent I magnitude of the FSRQ (upper panel) and BL Lac (bottom panel) blazars from the Roma-BZCAT (solid black lines) and blazar candidates identified in this work (dashed red lines).

WIBRaLS objects, signalling a single power-law character of their mid-IR emission continua, with mid-IR spectral indices roughly within a broad range of $0.5-2.0$ (see Table 3), consistently with the blazar classification. About half of our sample, however, is scattered much below the black dashed lines in the diagrams, indicating that their mid-IR emission continua are curved, with flatter slopes at longer wavelengths. This could be a signature of either a hot dust emission from host galaxies dominating the mid-IR output of the systems, or a non-negligible contamination of WISE fluxes by nearby foreground/background sources.

Subsequently, we investigated the IRAC colours of our blazar candidates using the $[3.6]-[4.5]-[8.0]$ μm and $[3.6]-[4.5]-[5.8]-[8.0]$ μm colour-colour diagrams, motivated by the supreme angular resolution of the IRAC instrument when compared to WISE ($\sim 2''$ versus $\sim 6''$). As shown in the resulting Figure 8, the IRAC colours of our blazar candidates are now more consistent with a single power-law character of their mid-IR emission continua, as expected for blazar sources, suggesting that a large scatter in the WISE colour-colour diagrams is mostly due to the contamination effect. Interestingly, we note that our sample is homogenous in that we do not see any clear separation between the FSRQ or the BL Lac blazar candidates. This may suggest that the majority of our BL Lac candidates are of the LBL type.

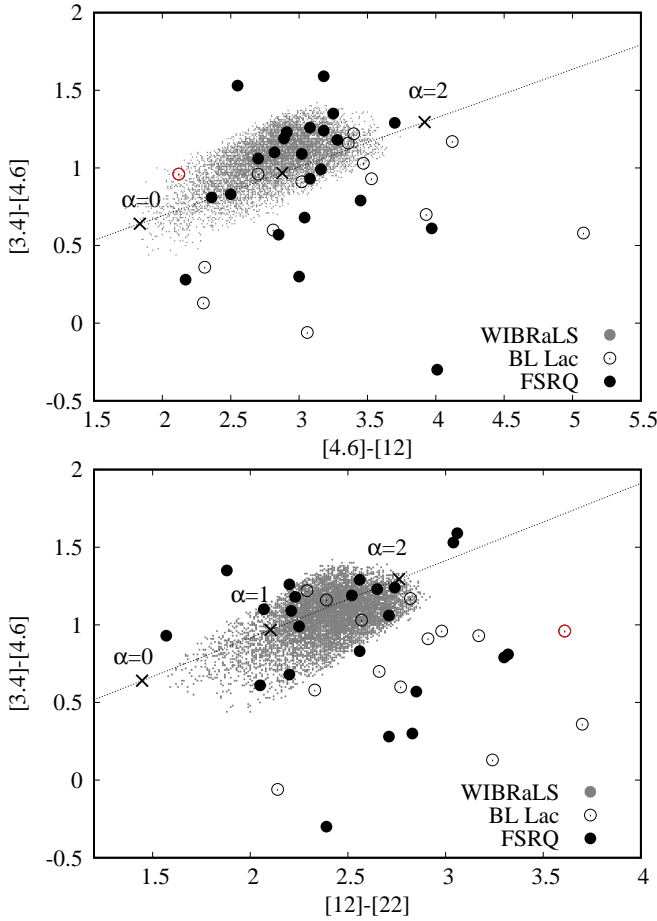


Figure 7. The WISE [3.4]-[4.6]-[12] (top panel) μm and [3.4]-[4.6]-[12]-[22] μm (bottom panel) colour-colour diagrams of OGLE blazar candidates. Open and filled black circles denote BL Lacs and FSRQs, respectively, while red open circles mark the BL Lac candidate J0545-6846; small grey dots stand for the γ -ray blazar candidates from WIBRaLS (D’Abrusco et al. 2014). Black dashed lines correspond to the case of a single power-law emission continuum within the entire range of wavelength considered (i.e., 3.4–12 μm in the upper panel, and 3.4–22 μm in the lower panel), with the particular values of mid-IR spectral indices $\alpha = 0, 1,$ and 2 denoted by \times symbols.

4.5. Radio polarization

Since the radio-optical emission of blazars is synchrotron in origin, a significant amount of polarization at radio and optical frequencies is expected. We therefore gathered all the available archival data for the linear radio degree PD_r and polarization angle (PA_r) from the AT20G catalogue and polarized flux density maps at 4.8 and 8.6 GHz for the LMC⁸ and SMC⁹ to investigate polarization properties for the selected blazar candidates in Tables 2 and 3. As a result, we extracted nine objects (see Table 4), out of which six are FSRQ and three are BL Lac blazar candidates; all of them are strongly polarized sources with $\text{PD}_r > 3\%$ at all the analyzed radio frequencies. These should be considered as “secure” blazar candidates.

The 4.8 and 5 GHz data were obtained with the same telescope but presumably on different dates. The fact that for the two objects, i.e., J0512-6732 and J0111-7302,

⁸ http://www.atnf.csiro.au/research/lmc_ctm/index.html

⁹ http://www.atnf.csiro.au/research/smc_ctm/index.html

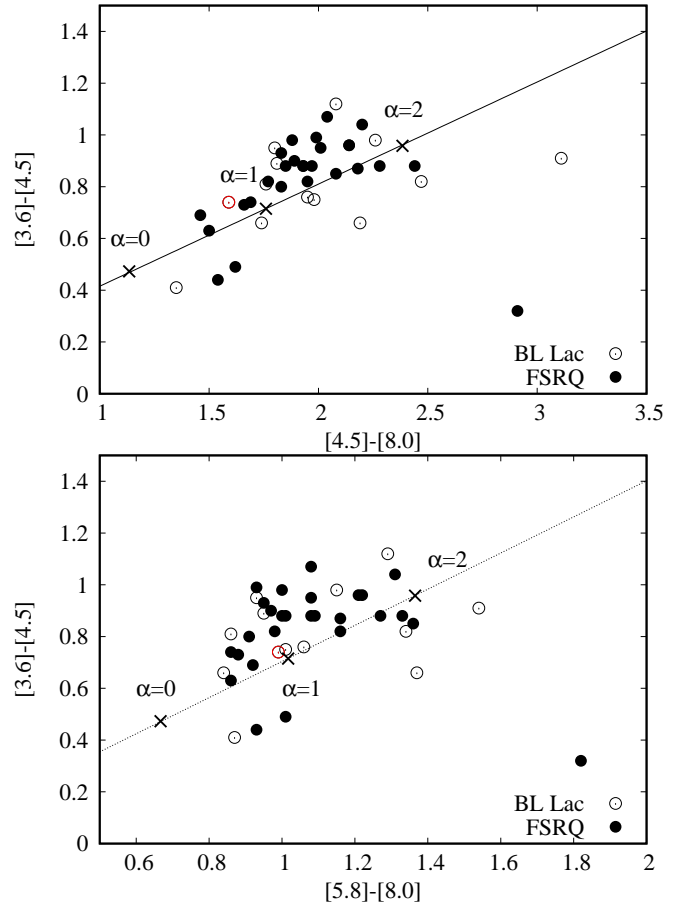


Figure 8. The IRAC [3.6]-[4.5]-[8.0] μm (top panel) and [3.6]-[4.5]-[5.8]-[8.0] μm (bottom panel) colour-colour diagrams of OGLE blazar candidates. Open and filled black circles denote BL Lacs and FSRQs, respectively, while red open circles mark the BL Lac candidate J0545-6846. Black dashed lines correspond to the case of a single power-law emission continuum within the entire range of wavelength considered (3.6–8.0 μm), with the particular values of mid-IR spectral indices $\alpha = 0, 1,$ and 2 denoted by \times symbols.

observed at both 4.8 and 5 GHz, there are very different PD_r in these close radio bands, suggests polarization variability, which is a further indication that they are blazar-like objects.

4.6. X-ray and γ -ray counterparts

We cross-matched our blazar candidates with the *Fermi* 2FGL catalogue (Nolan et al. 2012) and the ROSAT All-Sky Survey Catalogue (RASS-BSC; Voges et al. 1999) to search for their counterparts in γ - and X-ray regime. We did not find any match between the positions of our blazar candidates and the *Fermi* and RASS-BSC catalogues.

Recently, Ackermann et al. (2016a) reported the detection of four point-like sources in the area of the LMC. One of them is identified based on its characteristic pulsed γ -ray emission as pulsar PSR J0540–6919, while possible associations of the three remaining sources are still pending. None of these sources coincides with our blazar candidates.

Interestingly, Abdo et al. (2010a) noticed a flaring activity from the direction of LMC during the 4th month of the *Fermi*-LAT observations (at the turn of July and August 2008). The location of this event was es-

Table 4
The degree of linear polarization and polarization angle of FSRQ and BL Lac blazar type candidates.

Object	4.8 GHz	5 GHz	PD _r 8 GHz	8.6 GHz	20 GHz	4.8 GHz	PA _r	8.6 GHz
(1)	[%]	[%]	[%]	[%]	[%]	[°]		[°]
(2)	(3)	(4)	(5)	(6)	(7)	(8)		(8)
FSRQs								
J0114–7320	9.5±0.5			7.0		70.7±14.7		−12.9±14.3
J0120–7334	5.0±0.3					−52.2±0.7		
J0442–6818		11.7	10.0		8.1			
J0512–6732	3.3±0.2	12.7	10.7		13.6	13.6±2.1		
J0551–6916	7.3±0.4					8.3±38.2		
J0551–6843	9.1±0.5					−3.9±40.4		
BL Lacs								
J0111–7302	4.1±0.2	8.3	8.3		9.7	4.7±34.1		
J0501–6653	10.6±0.5			22.7±1.1		−2.8±25.6		−11.1±46.1
J0518–6755 ^a	12.6±0.6					−16.6±11.0		

Note. — ^aDubious; Columns: (1) source designation, (2)-(6) linear polarization degree (PD_r) at 4.8, 5, 8, 8.6, and 20 GHz, (7)-(8) linear polarization angle (PA_r) at 4.8 GHz and 8.6 GHz.

timated by fitting a point source with the 2DG model and HII gas map as templates for the LMC emission to the datasets. Using the 2DG model, the source was found at RA = 05^h46^m2 and DEC = −69°01′ with a detection significance of 4.5σ and 36′ containment radius, while with the HII map, at the position of RA = 05^h46^m4 and DEC = −69°01′, with 4.6σ significance and 29′ radius. In Figure 1 (top panel), we show both possible locations of the flaring activity (green circle denotes the 2DG model and black circle – H II gas map) which, moreover, coincide with positions of four our blazar candidates, namely J0545–6846, J0551–6843, J0551–6916, and J0552–6850. The BL Lac candidate J0545–6846, for which the broad-band SED is shown in Figure 9, is consistent with both estimated locations, and is characterized by a particularly large radio flux and high radio-loudness in our sample. We however note here a rather large integrated flux > 1 GeV of the LAT transient, $\simeq 9.6^{+2.8}_{-6.1} \times 10^{-12} \text{ erg s}^{-1} \text{ cm}^{-2}$; if related to the flaring activity of J0545–6846, this would imply an unusually large value of the Compton dominance parameter as for a BL Lac candidate.

The *Fermi* group noticed also the second γ -ray event, which took place a few years later, in April 2015. It is not

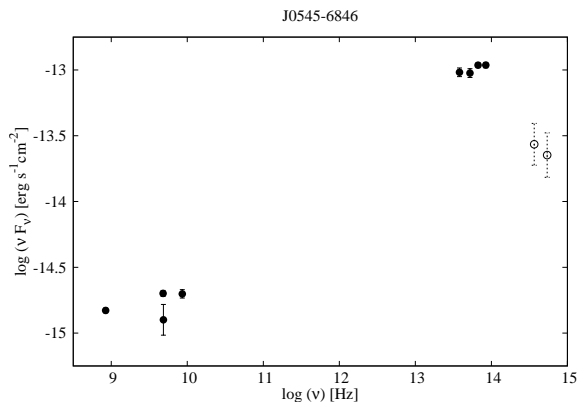


Figure 9. SED of the J0545–6846 BL Lac candidate, which coincides with the γ -ray transient detected by the *Fermi*-LAT; open circles denote optical data from the FS list, black filled circles are for the archival radio and mid-IR data.

clear if the two flares are produced by the same object, but they originated from about the same direction. The source, however, did not show up in a full six-year data analysis.

4.7. Identification procedure: a summary

Figure 10 shows the radio contours overlaid on the grey scale optical images for the blazar candidates identified in the OGLE data for the LMC and the SMC. We used the Digitized Sky Survey (DSS) R band optical images as grey scales and the radio data at 8.6, 4.85 or 0.845 GHz as contours. A black cross marks the optical position from the MQS catalogue or the FS list for each blazar candidate. All the sources which were found in the PMN catalogue only, as well as other sources which are not associated with the strongest central radio emission indicated by the radio contours, are considered as dubious and marked with the “a” symbol in Tables 2 and 3. The main results of our further analysis of the selected blazar candidates are:

1. As a result of the cross-matching procedure, we selected a sample of 44 objects, including 27 FSRQ and 17 BL Lac blazar candidates. This significantly increased the sample of blazar candidates behind LMC and SMC.
2. Each selected object is optically faint with the I band magnitude between 16 and 21.
3. All the FSRQ candidates are distant sources with redshifts from 0.286 up to 3.320. The redshift distribution for BL Lacs is unknown due to the lack of lines in their optical spectra.
4. The radio-loudness parameter R varies from 12 to 4,450 for the FSRQ blazar candidates and from 171 to 7,020 for the BL Lac candidates, implying that all the sources included in the sample are radio-loud indeed.
5. The estimated values of the radio spectral index α_r vary from −0.57 to 1.37. Since we used non-simultaneous archival radio data in the analysis,

the α_r may indicate radio flux variability for the sampled sources, as expected for blazars, rather than steep radio spectra.

6. The infrared colours indicate that the infrared continua of the selected sources are non-thermal in origin, as expected for blazars. The estimated values of mid-IR spectral indices for the majority of sources are between 0.5 and 2.0.
7. The PD_r and PA_r were found in the AT20G catalogue or were measured by us from the archival radio maps of the 4.8 and 8.6 GHz surveys of the LMC and SMC. All the blazar candidates listed in the Table 4 are strongly polarized sources with the average polarization of $PD_{r,4.8} \sim 6.8\%$ at 4.8 GHz.
8. Although we did not find any clear associations with high-energy γ -ray emitters, we note a repeating flaring activity detected with *Fermi*-LAT from the direction of the J0545–6846 BL Lac candidate.

5. DISCUSSION: RELEVANCE OF THE ANALYSIS

5.1. Physics of blazar sources

The majority of blazars of the FSRQ and LBL types are identified in the radio surveys (e.g., [Stickel et al. 1991](#); [Perlman et al. 1996, 1998](#); [Caccianiga et al. 2002](#)), while HBLs are mostly discovered via the X-ray surveys (e.g., [Pursimo et al. 2013](#); [Rector et al. 2000](#); [Landt et al. 2001](#), but see [Plotkin et al. 2010](#) for the optically selected BL Lac sample using the SDSS data). This naturally leads to various selection biases, as any flux-limited survey will detect sources which are the brightest in a given frequency band. As an illustration of the problems arising in this context one can note that the luminosity evolution of the radio-selected BL Lacs was previously claimed to be different from that of the X-ray-selected BL Lacs, the finding which was however not confirmed in the follow-up studies using larger samples (e.g., [Padovani et al. 2007](#), and references therein). Our blazar candidates are selected uniquely from the deep, flux-limited optical survey, based on the *time-domain* analysis, and as such could in principle be of relevance for in-depth population studies of blazar sources.

We also emphasize here the optical variability of blazars on different timescales, which was and is a subject of an intense research, albeit typically limited to rather small and sparse samples of sources (e.g., [Webb et al. 1988](#); [Ghosh et al. 2000](#)). Although the variable optical emission of blazars originates predominantly in nuclear relativistic jets, it may also contain a pronounced contribution from accretion disks, which are modulating the jet activity, as seen directly in a few luminous radio galaxies and quasars ([Lohfink et al. 2013](#); [Bhatta et al. 2018](#)). Interestingly, all the newly identified blazar candidates in our sample have high photometric accuracy, high cadence optical light curves from the long-term (~ 2 decades) photometric monitoring from OGLE (OGLE-III and OGLE-IV phases).

5.2. MC magnetic field study

Since magnetic field may play an important role in the cosmological evolution of galaxies, it is mandatory

to disclose in detail its origin, structure and strength in nearby galaxies, including the nearest dwarf galaxies, i.e., the SMC and LMC. The commonly used method for investigating the galactic magnetic field morphology, is the Faraday rotation measure (RM) study of background polarized sources (as implemented by, e.g., [Brun 1966](#); [Kawabata et al. 1969](#), or more recently [Brentjens & de Bruyn 2005](#)). In this way, the magnetic field of the MCs system, i.e., the SMC, LMC, and Magellanic Bridge (MB), was intensively investigated in a last few decades, first using the optical ([Schmidt 1970](#); [Mathewson & Ford 1970](#)) and then radio data (e.g., [Haynes et al. 1986](#); [Klein et al. 1993](#); [Gaensler et al. 2005](#); [Mao et al. 2012](#); [Kaczmarek et al. 2017](#)). Our sample of blazar candidates should be therefore relevant in this context as well, as it identifies potentially *variable* polarized emitters behind the MCs system, which should be treated with caution when included in the RM studies.

5.3. γ -ray study

One of the key projects of the newly emerging very high energy γ -ray observatory Cherenkov Telescope Array (CTA), is to conduct a deep LMC survey, expanding over previous results provided by the currently operating γ -ray observatories, namely *Fermi*-LAT and H.E.S.S. (see Chapter 7 in [Acharya et al. 2017](#)). This project will allow to study in detail the diffuse γ -ray emission of the LMC, including processes of cosmic ray acceleration and propagation within the interstellar medium, but also enabling the dark matter research. Clearly, a proper identification of all the potential background γ -ray emitters behind the MC system, i.e., blazars, is indispensable for a correct analysis and interpretation of the γ -ray data on the LMC in general, and the planned CTA observations in particular.

We thank Dr Pierrick Martin and Dr Shane O’Sullivan for fruitful discussions and comments on the analysis. NŻ work was supported by the Polish National Science Centre (NCN) through the grant DEC-2014/15/N/ST9/05171. AG and MO acknowledge support from the NCN through the grant 2012/04/A/ST9/00083. AG also acknowledges partial support from 2013/09/B/ST9/00026. LS was supported by Polish NSC grant 2016/22/E/ST9/00061. The OGLE project has received funding from the NCN MAESTRO grant no.2014/14/A/ST9/00121 to AU. SK also acknowledges the financial support from the NCN OPUS grant no. 2014/15/B/ST9/00093.

REFERENCES

- Abdo, A. A., et al. 2010a, *A&A*, 512, A7
 —. 2010b, *ApJ*, 715, 429
 Acharya, B. S., et al. 2017, *ArXiv e-prints*
 Ackermann, M., et al. 2016a, *A&A*, 586, 17
 —. 2016b, *ApJ*, 824, L20
 —. 2017, *ApJ*, 837, L5
 Aharonian, F., et al. 2007, *ApJ*, 664, L71
 Aller, M. F., Aller, H. D., & Hughes, P. A. 2003, *ApJ*, 586, 33
 Angel, J. R. P., & Stockman, H. S. 1980, *ARA&A*, 18, 321
 Begelman, M. C., Blandford, R. D., & Rees, M. J. 1984, *Reviews of Modern Physics*, 56, 255
 Bhatta, G., et al. 2018, *ArXiv e-prints*
 Blandford, R. D., & Königl, A. 1979, *ApJ*, 232, 34
 Blinov, D. A. nad Hagen-Thorn, V. A. 2009, *A&A*, 503, 103

- Bock, D. C.-J., Large, M. I., & Sadler, E. M. 1999, *AJ*, 117, 1578
- Bolatto, A. D., Simon, J. D., Stanimirović, S., van Loon, J. T., Shah, R. Y., Venn, K., & Leroy, A. K. 2007, *ApJ*, 655, 212
- Bothun, B. D., & Thompson, I. B. 1988, *AJ*, 96, 877
- Böttcher, M., Reimer, A., Sweeney, K., & Prakash, A. 2013, *ApJ*, 768, 54
- Brentjens, M. A., & de Bruyn, A. G. 2005, *A&A*, 441, 1217
- Brun, B. J. 1966, *MNRAS*, 133, 67
- Caccianiga, A., Marchà, M. J., Antón, S., Mack, K.-H., & Neeser, M. J. 2002, *MNRAS*, 329, 877
- Cui, W. 2004, *ApJ*, 605, 662
- Cutri, R. M., et al. 2013, Explanatory Supplement to the AllWISE Data Release Products, Tech. rep.
- D’Abrusco, R., Massaro, F., Ajello, M., Grindlay, J. E., Smith, H. A., & Tosti, G. 2012, *ApJ*, 748, 68
- D’Abrusco, R., Massaro, F., Paggi, A., Smith, H. A., Masetti, N., Landoni, M., & Tosti, G. 2014, *ApJS*, 215, 14
- Dickel, J. R., Gruendl, R. A., McIntyre, V. J., & Amy, S. W. 2010, *AJ*, 140, 1511
- Dickel, J. R., McIntyre, V. J., Gruendl, R. A., & Milne, D. K. 2005, *AJ*, 129, 790
- Fan, J.-H., et al. 2008, *PASJ*, 5, 707
- Filipović, M. D., Bohlson, T., Reid, W., Staveley-Smith, L., Jones, P. A., Nohejl, K., & Goldstein, G. 2002, *MNRAS*, 335, 1085
- Fossati, G., Maraschi, L., Celotti, A., Comastri, A., & Ghisellini, G. 1998, *MNRAS*, 299, 433
- Gaensler, B. M., Haverkorn, M., Staveley-Smith, L., Dickey, J. M., McClure-Griffiths, N. M., Dickel, J. R., & Wolleben, M. 2005, *Sci*, 307, 1610
- Ghisellini, G., Celotti, A., Fossati, G., Maraschi, L., & Comastri, A. 1998, *MNRAS*, 301, 451
- Ghisellini, G., Haardt, F., Della Ceca, R., Volonteri, M., & Sbarrato, T. 2013, *MNRAS*, 432, 2818
- Ghisellini, G., & Tavecchio, F. 2008, *MNRAS*, 387, 1669
- Ghisellini, G., Tavecchio, F., Maraschi, L., Celotti, A., & Sbarrato, T. 2014, *Nature*, 515, 376
- Ghosh, K. K., Ramsey, B. D., Sadun, A. C., & Soundararajaperumal, S. 2000, *ApJS*, 127, 11
- Gordon, K. D., et al. 2011, *AJ*, 142, 102
- Griffith, M. R., & Wright, A. E. 1993, *AJ*, 105, 1666
- Haberl, F., Filipović, M. D., Pietsch, W., & Kahabka, P. 2000, *Astronomy and Astrophysics Supplement*, 142, 41
- Haberl, F., & Pietsch, W. 1999, *Astronomy and Astrophysics Supplement*, 139, 277
- Haynes, R. F., Murray, J. D., Klein, U., & Wielebinski, R. 1986, *A&A*, 159, 22
- Ho, L. C. 2002, *ApJ*, 564, 120
- Iler, A. L., Schachter, J. F., & Birkinshaw, M. 1997, *ApJ*, 486, 117
- Jorstad, S. G., Marscher, A. P., Stevens, J. A., Smith, P. S., & Forster, J. R. 2007, *AJ*, 134, 799
- Kaczmarek, J. F., Purcell, C. R., Gaensler, B. M., & McClure-Griffiths, N. M. 2017, *MNRAS*, 467, 1776
- Kawabata, K., Fujimoto, M., Sofue, Y., & Fukui, M. 1969, *PASJ*, 21, 293
- Kellermann, K. I., Sramek, R., Schmidt, M., Shaffer, D. B., & Green, R. 1989, *AJ*, 98, 1195
- Kelly, B. C., Bechtold, J., & Siemiginowska, A. 2009, *ApJ*, 698, 895
- Klein, U., Haynes, R. F., Wielebinski, R., & Meinert, D. 1993, *A&A*, 271, 402
- Kozłowski, S. 2016, *ApJ*, 826, 118
- Kozłowski, S., & Kochanek, C. S. 2009, *ApJ*, 701, 508
- Kozłowski, S., Kochanek, C. S., & Udalski, A. 2011, *ApJS*, 194, 22
- Kozłowski, S., et al. 2010, *ApJ*, 708, 927
- . 2012, *ApJ*, 746, 27
- . 2013, *ApJ*, 775, 92
- Landt, H., Padovani, P., Perlman, E. S., Giommi, P., Bignall, H., & Tzioumis, A. 2001, *MNRAS*, 323, 757
- Lohfink, A. M., et al. 2013, *ApJ*, 772, 83
- Mao, S. A., et al. 2012, *ApJ*, 759, 25
- Marscher, A. P. 2014, *ApJ*, 780, 87
- Massaro, E., Maselli, A., Leto, C., Marchegiani, P., Perri, M., Giommi, P., & Piranomonte, S. 2015, *Ap&SS*, 357, 75
- Massaro, F., D’Abrusco, R., Ajello, M., Grindlay, J. E., & Smith, H. A. 2011, *ApJ*, 740, L48
- Massey, F. J. J. 1951, *Journal of the American Statistical Association*, 46, 68
- Mathewson, D. S., & Ford, V. L. 1970, *ApJ*, 160, L43
- McConnell, D., Sadler, E. M., Murphy, T., & Ekers, R. D. 2012, *MNRAS*, 422, 1527
- Meixner, M., et al. 2006, *AJ*, 132, 2268
- Murphy, T., et al. 2010, *MNRAS*, 402, 2403
- Nolan, P. L., et al. 2012, *ApJS*, 199, 31
- Padovani, P., Giommi, P., Landt, H., & Perlman, E. S. 2007, *ApJ*, 662, 182
- Perlman, E. S., Padovani, P., Giommi, P., Sambruna, R., Jones, L. R., Tzioumis, A., & Reynolds, J. 1998, *AJ*, 115, 1253
- Perlman, E. S., et al. 1996, *ApJS*, 104, 251
- Plotkin, R. M., et al. 2010, *AJ*, 139, 390
- Pursimo, T., et al. 2013, *ApJ*, 767, 14
- Rector, T. A., Stocke, J. T., Perlman, E. S., Morris, S. L., & Gioia, I. M. 2000, *AJ*, 120, 1626
- Schmidt, T. 1970, *A&A*, 6, 294
- Stern, D., et al. 2005, *ApJ*, 631, 163
- Stickel, M., Padovani, P., Urry, C. M., Fried, J. W., & Kuehr, H. 1991, *ApJ*, 374, 431
- Stocke, J. T., Morris, S. L., Weymann, R. J., & Foltz, C. B. 1992, *ApJ*, 396, 487
- Tarnopolski, M. 2015, *MNRAS*, 454, 1132
- Udalski, A., et al. 2008a, *AcA*, 58, 89
- . 2008b, *AcA*, 58, 329
- Urry, C. M., & Padovani, P. 1995, *PASP*, 107, 803
- Voges, W., et al. 1999, *A&A*, 349, 389
- Webb, J. R., Smith, A. G., Leacock, R. J., Fitzgibbons, G. L., Gombola, P. P., & Shepherd, D. W. 1988, *AJ*, 95, 374
- Werner, M. W., et al. 2004, *ApJS*, 154, 1
- Wright, A. E., Griffith, M. R., Burke, B. F., & Ekers, R. D. 1994, *ApJS*, 91, 111
- Wright, E. L., et al. 2010, *AJ*, 140, 1868
- Zhang, H., Deng, W., Li, H., & Böttcher, M. 2016, *ApJS*, 817, 63

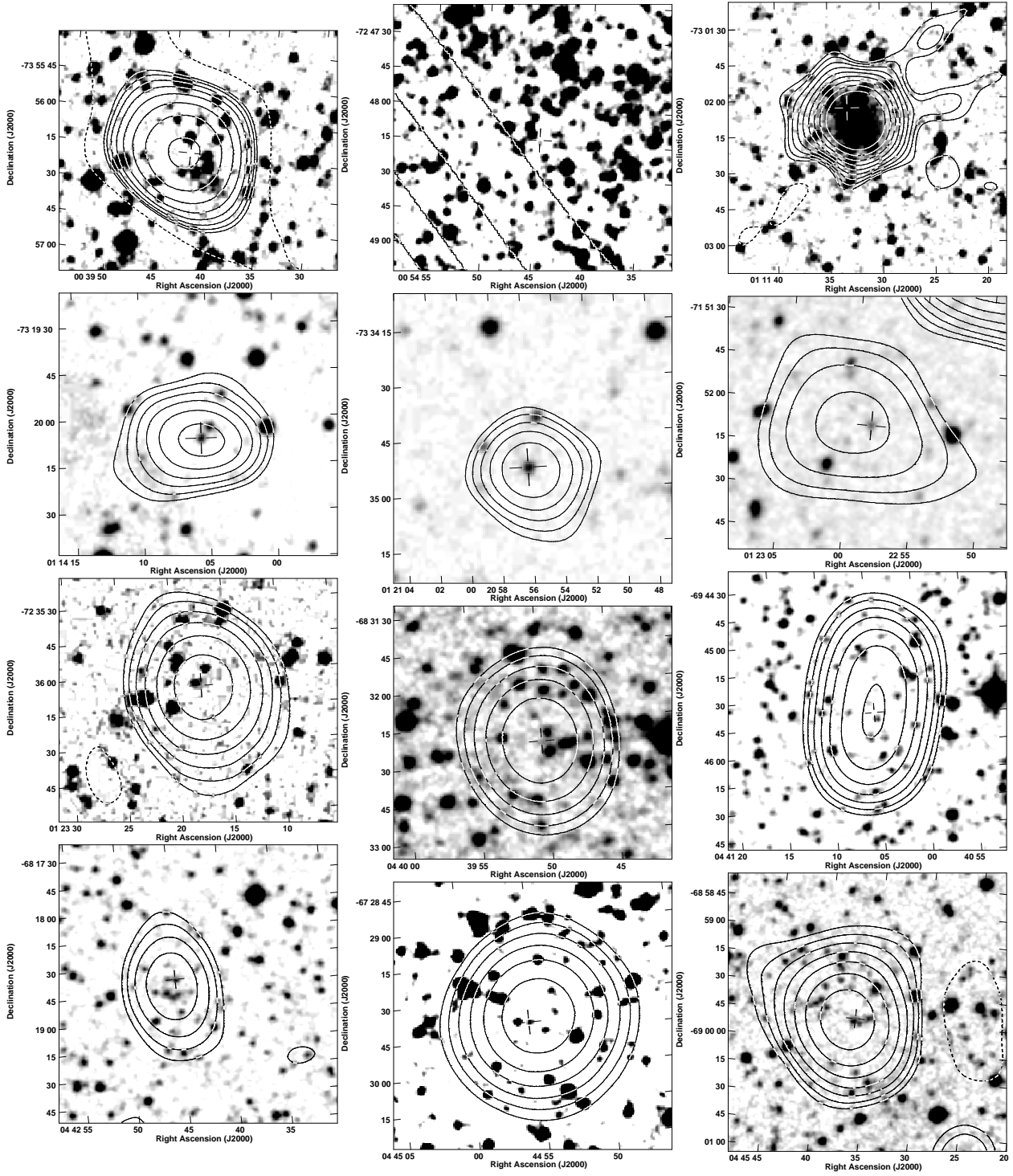


Figure 10. Contour maps of all sampled blazar candidates. The contour maps were created with DSS-R band optical images (greys) and 8.6, 4.85 or 0.845 GHz radio data (contours). A black cross marks the blazar candidate optical position from the MQS catalogue or the FS list.

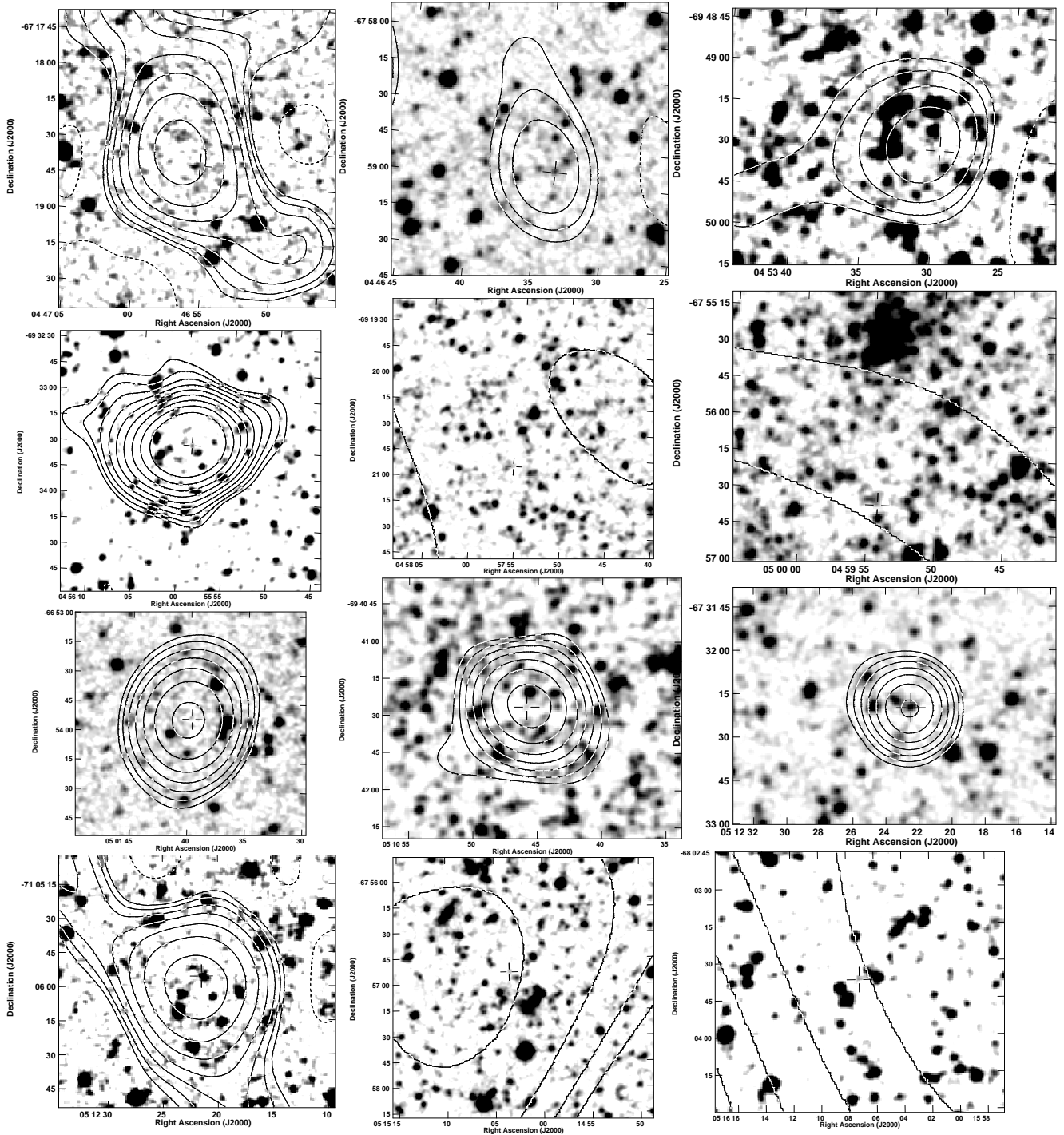


Figure 10. Continued.

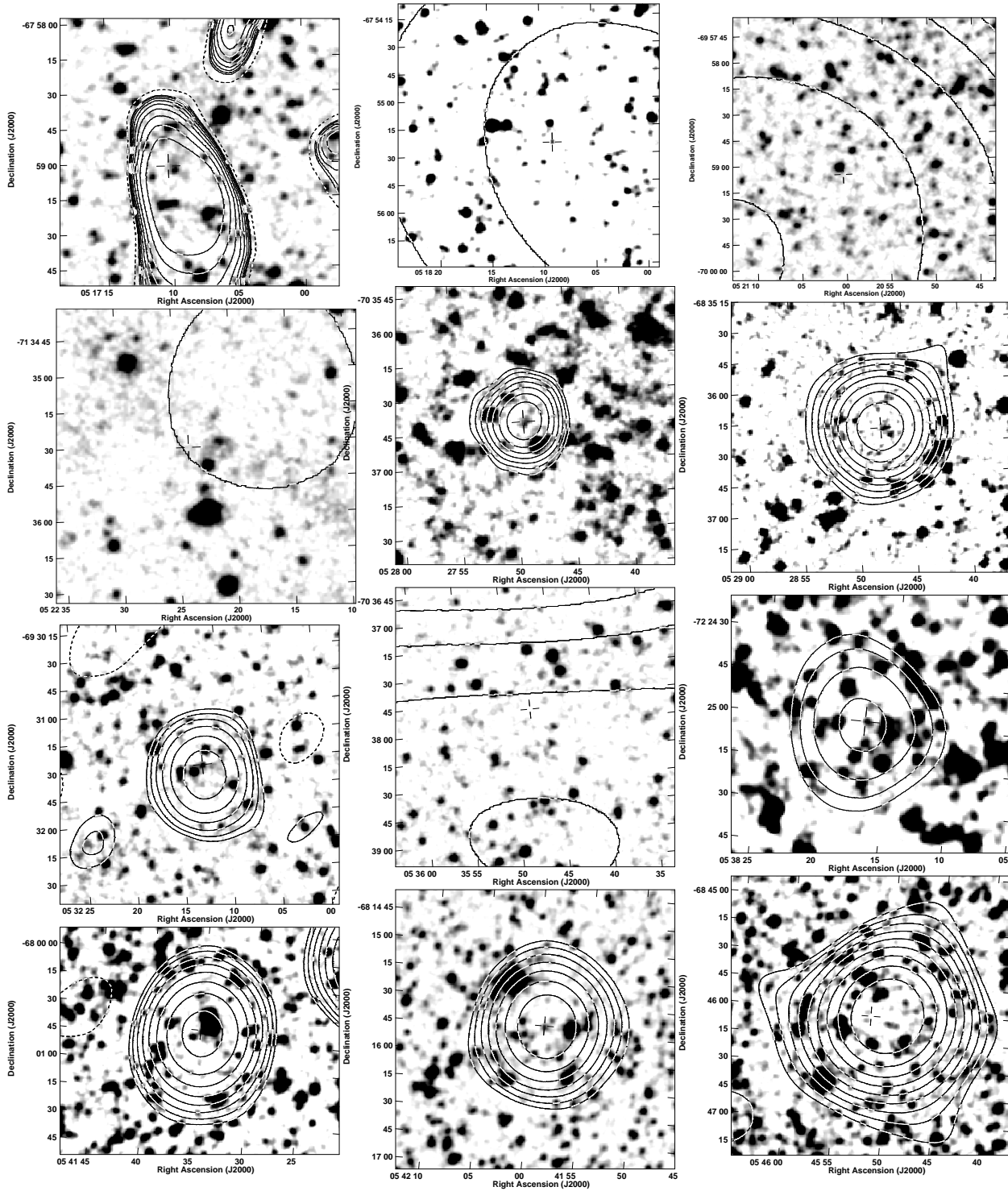


Figure 10. Continued.

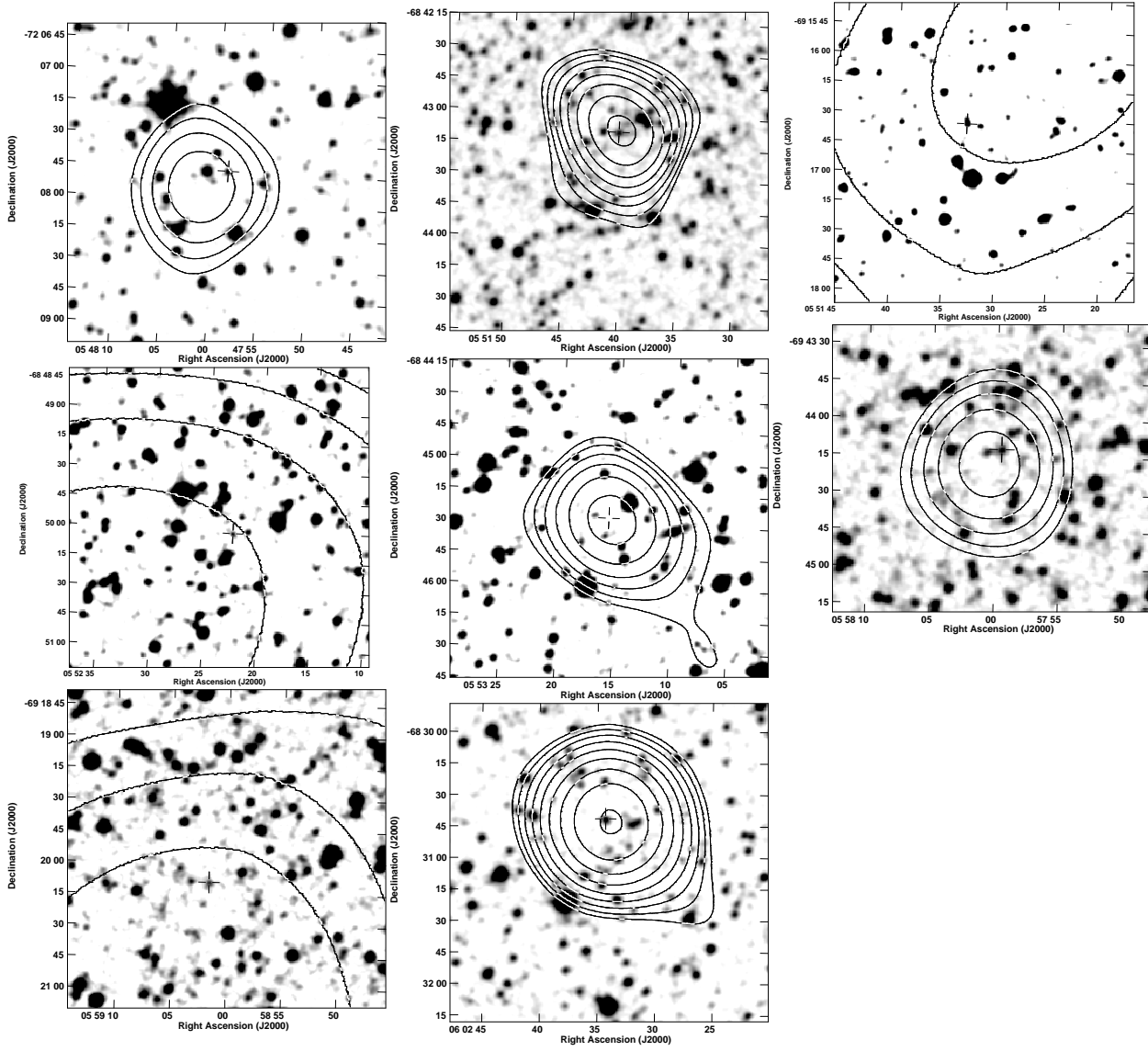


Figure 10. Continued.